Thin Solid Films 707 (2020) 138098

Contents lists available at ScienceDirect

Thin Solid Films

journal homepage: www.elsevier.com/locate/tsf

Effects of lithium doping and ultraviolet photo-patterning on electrical properties of InGaZnO thin film transistors

Jongsu Jang, Yongtaek Hong*

Department of Electrical and Computer Engineering, Inter-University Semiconductor Research Center (ISRC), Seoul National University, Seoul 08826, Republic of Korea

ARTICLE INFO

Keywords:
Lithium doping
Ultraviolet photo-patterning
Solution-process
Thin film transistors
Indium gallium zinc oxide

ABSTRACT

Alkali metals, such as Li and Na, have been added in solution-processed oxide thin-film transistors (TFTs) because they improved electrical characteristics of the oxide TFTs. In previous research, however, fine-patterning of the alkali metal-doped oxide layers was not performed due to potential performance degradation during photolithography process. In this work, we demonstrate ultraviolet (UV) photo-patterned solution-processed indium gallium zinc oxide (IGZO) TFTs containing various amount of lithium (Li). For patterning of active layer, we applied deep UV (184 nm, 10% and 254 nm, 90%) photo-patterning process. We also investigated the chemical composition and bonding structures of the Li doped IGZO (Li-IGZO) films. It was found that appropriate Li doping on IGZO films can reduce oxygen vacancies and improved the coordination of the metal-oxygen bonding. In addition, Li-IGZO TFTs showed improved mobility and bias stability compared to un-doped counterparts. We believe that this simple patterning process and Li doping can be applied to other types of the high-performance solution-processed oxide TFTs.

1. Introduction

Recently, flat panel displays have been intensively developed for the higher resolution and larger screen size. For these applications, metal oxide semiconductors, such as indium gallium zinc oxide (IGZO), zinc tin oxide and indium oxide, has been considered as one of the most promising materials due to their high carrier mobility and facile scalability [1–5]. Among these metal-oxide based materials, IGZO thin film transistors (TFTs) have been used in the backplane of commercial display products because of its relatively high field effect mobility and good stability. In addition, solution-processed oxide semiconductors have much attention owing to the simple and low-cost processes. However, solution-processed oxide TFTs have shown relatively low performance in comparison with their vacuum deposition counterpart [6].

To overcome this disadvantage, many research group have been studied to enhance the performance of the TFTs. By adding or controlling the composition of metal ion such as Ga, Hf, In and Sn, they suppress defect levels or enhance 5s-orbitals overlap to form electron-transporting paths [7–10]. Alkali metal ions also have been investigated as an enhancer to obtain high performance solution-processed oxide semiconductors. Among the alkali metal, lithium (Li) has a low standard electrode potential value (-3.04 V) and a high binding energy with oxygen ions [11]. In addition, Li ion, the smallest metal than others, easily occupy the interstitial sites and release free electrons [12]. We reported the Li doping can improve the performance of ZnO TFTs [13]. In addition, many groups have reported alkali metals doped oxide TFTs due to their high mobility and good electrical stability for solution-processed oxide TFTs [13–18]. However, most of the Li doped metal oxide TFTs showed the transfer characteristics in the saturation region because of their non-patterned active layer.

As another approach to overcoming low electrical performance and high annealing temperature of solution-processed oxide TFTs, a photochemical activated oxide films including semiconductors and dielectrics were reported [19,20]. This photochemical activation process also gives an opportunity of patterning in the solution-processed metal oxide thin film [21–24]. Although additive patterning methods such as ink-jet and electrohydrodynamic printing are good for low-cost deposition process, it still has difficulty for controllability of the uniformity and thickness of the thin film. In comparison to printing technique, direct ultraviolet (UV) photo-pattering could pattern the uniform thin films and enhance the metal oxide formation [21].

In this work, we investigated the effects of Li doping on the electrical characteristics of solution-processed IGZO TFTs. In addition, the feasibility of UV photo-patterning for Li doped IGZO (Li-IGZO) TFTs were studied. The pattering of semiconductor layers is important to

* Corresponding author.
E-mail addresses: jongsu@snu.ac.kr (J. Jang), yongtaek@snu.ac.kr (Y. Hong).

https://doi.org/10.1016/j.tsf.2020.138098
Received 15 December 2019; Received in revised form 1 May 2020; Accepted 1 May 2020
Available online 18 May 2020
0040-6090/ © 2020 Elsevier B.V. All rights reserved.

reduce leakage current and crosstalk noise [25,26]. However, owing to the porous structures of the solution processed oxide thin films, the chemicals such as photoresist stripper spread through the film during the photolithography process and thus can degrade the semiconductor performance [27,28]. It is noted that most of the previous studies on the Li (or alkali metal) doped solution-processed oxide TFTs used non-patterned channel layer and thus the transfer characteristics only in the saturation region were shown [13–15,17,18]. It is also noted that the high-quality transfer characteristics in linear region are difficult to be obtained due to high leakage and noise properties if the semiconductor layer is not patterned. We used deep UV photo-patterning process, which does not need toxic chemicals such as photoresists, developers, and photoresist strippers. No damage to the alkali metal-doped oxide thin film has been observed. The chemical compositions and bonding structures of the Li-IGZO films were investigated by glancing X-ray diffraction and X-ray photoelectron spectroscopy. Li doping and UV photo-patterning finally improved the electrical properties and bias stability of Li-IGZO TFTs.

2. Experimental details

In this work, we prepared two kinds of precursor solutions: one with acetate salts (type-A precursors) and the other with nitrate salts (type-B precursors) for indium an gallium elements. Based on our experience, type-B precursors showed results less sensitive to environment conditions during the fabrication process and did not need stabilizer in comparison with the precursor based on acetate salts. In addition, we fabricated devices for UV photo-patterning experiment with type-B precursors in Ar ambient glove box for further eliminating environment dependency and reliable patterning repeatability while devices for Li-doping effect analysis were fabricated with type-A precursors in air. After 10 min hotplate annealing at 150 °C in air and Ar ambient for type-A and type-B precursors, respectively, the final annealing at high temperatures (350 or 450 °C) were performed in furnace under environment conditions for both precursors. All chemicals were purchased from the Sigma-Aldrich. The mole ratio of In: Ga: Zn was fixed at 3: 1: 2. The total metal ion concentration of the In, Ga, and Zn maintained at 0.2 M in 2-methoxyethanol ($CH_3OCH_2CH_2OH$). The Li concentration (Li/(In + Ga + Zn)) was obtained 0 % to 25 % by dissolving Li salts in the precursor solutions. The type-A precursor solutions were prepared by dissolving indium acetate ($In(C_2H_3O_2)_3$), gallium nitrate hydrate ($Ga(NO_3)_3{\cdot}xH_2O$), zinc acetate dihydrate ($Zn(CH_3COO){\cdot}2H_2O$), and lithium chloride (LiCl) in 2-methoxyethanol. The 0.2M ethanolamine ($NH_2CH_2CH_2OH$) was added as a stabilizer to the mixture. The type-B precursor solutions for UV photo-patterning process were prepared by dissolving indium nitrate hydrate ($In(NO_3)_3{\cdot}xH_2O$), gallium nitrate hydrate ($Ga(NO_3)_3$) $\cdot xH_2O$), zinc nitrate hexahydrate ($Zn(NO_3)_2{\cdot}6H_2O$), and lithium nitrate ($LiNO_3$) were dissolved in 2-methoxyethanol. The acetylacetone ($CH_3COCH_2COCH_3$) was added to the mixture with 0.1 M concentration. Each precursor solution was stirred vigorously at 80 °C for 2 h.

The Li-IGZO films were deposited on heavily boron doped p-type silicon wafer substrates with a 200 nm silicon dioxide (SiO_2) layer, which act as gate electrode and gate dielectric layer, respectively. Before spin coating, the cleaned substrates were exposed to UV light for 10 min. For type-A TFTs fabricated with the type-A precursor solution, Li-IGZO films were spin-coated at 4000 rpm for 30 s in air. The films dried on a hotplate at 150 °C for 10 min and then annealed at 400 °C furnace for 1 h in air. For type-B TFTs fabricated with the type-B precursor and whose semiconductor layer was UV photo-patterned, Li-IGZO films were spin-coated at 3000 rpm for 30 s and dried at 150 °C hotplate for 10 min. Both spin coating and film drying were performed in argon (Ar) ambient glove box for further eliminating external environmental factors. Next, the Li-IGZO films were exposed to the deep ultraviolet light (184 nm, 10%; 254 nm, 90%) through the shadow mask for 30 min in air atmosphere for patterning and metal-oxide formation. After the UV exposure, unreacted oxide thin films were removed with methanol and acetic acid mixture (20 mL: 1 mL) and after that, the samples were rinsed in deionized (DI) water. Finally, the patterned Li-IGZO films were annealed at desired temperatures (350–450 °C) for 2 h in air. Finally, aluminum source and drain (S/D) electrodes of thickness 100 nm were thermally evaporated on IGZO thin-films. The channel region was defined with a width of 1000 µm and length was varied from 100 to 200 µm. In case of the Li-IGZO TFTs using type-A precursors, the active semiconductor layers were mechanically isolated or patterned with hard probe tips before electrical measurements in order to reduce any leakage current from the non-patterned oxide semiconductor layer.

The electrical characteristics of the fabricated TFTs were analyzed using an Agilent 4155C semiconductor parameter analyzer at room temperature in a dark box and air atmosphere. All transfer curves were obtained by sweeping the gate voltage from negative to positive values. We observed counterclockwise hysteresis for all transfer curves, which was further reduced with Li doping. The glancing XRD was performed with a high-resolution X-ray diffractometer (PANalytical, X'Pert PRO) with Cu Kα radiation (ω = 0.5°). The X-ray photoelectron spectroscopy (XPS) analysis for the Li-IGZO films was carried out by an AXIS-HSi (KRATOS) XPS instrument using Al Kα source (1486.7 eV). The binding energy of the XPS spectra was calibrated by the C 1s peak (284.5 eV). The XPS peak fitting was carried out by using a CasaXPS software. The O 1s peaks were fitted using the Gaussian distributions, which included prior iterative Shirley background subtraction.

3. Results and discussion

In order to analyze the crystallinity of the Li-IGZO films SiO_2/Si wafer substrates, we measured glancing XRD of the Li-IGZO films as shown in Fig. 1 because general XRD data do not clearly show small peaks due to the very high Si peak. There are peaks at 51.66°, 53.94°, and 55.30° (2theta) in all samples. It is found that Li doping does not change the lattice structure of the IGZO. In case of the Si (100) wafer, the (311) planes are oriented at approximately 55° (2theta) from the wafer surface. The one set of planes often shows up between 50 and 55 in glancing XRD measurements. Thus, we could infer that Li-IGZO films have no crystalline structure. In contrast to our previous research about Li doped ZnO films [13], which showed crystallinity properties, the IGZO films have no orientation regardless of Li doping up to 25%. This indicates that IGZO and Li-IGZO films are amorphous phase. It is reported that ZnO-like films can be obtained when Zn content is over 87 at.% in In-Ga-Zn-O system [29].

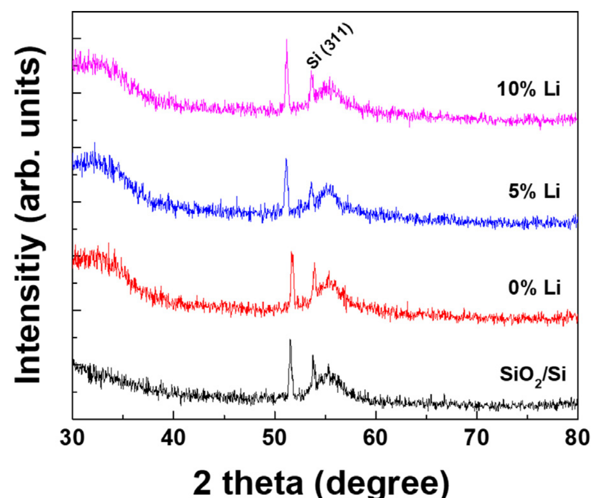

Fig. 1. Glancing XRD patterns of the UV photo-patterned Li-IGZO films annealed at 450 °C.

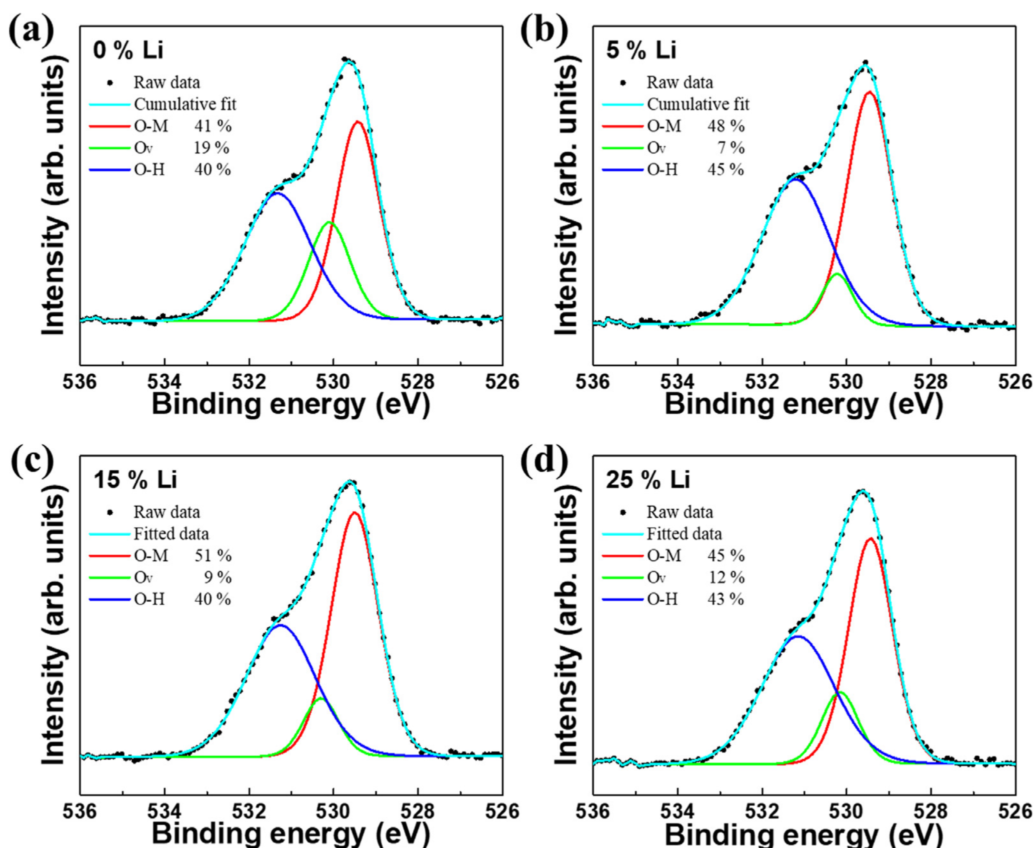

Fig. 2. XPS O 1s peak of the Li-IGZO films with various Li concentrations (a) 0 %, (b) 5 %, (c) 15 %, and (d) 25 %.

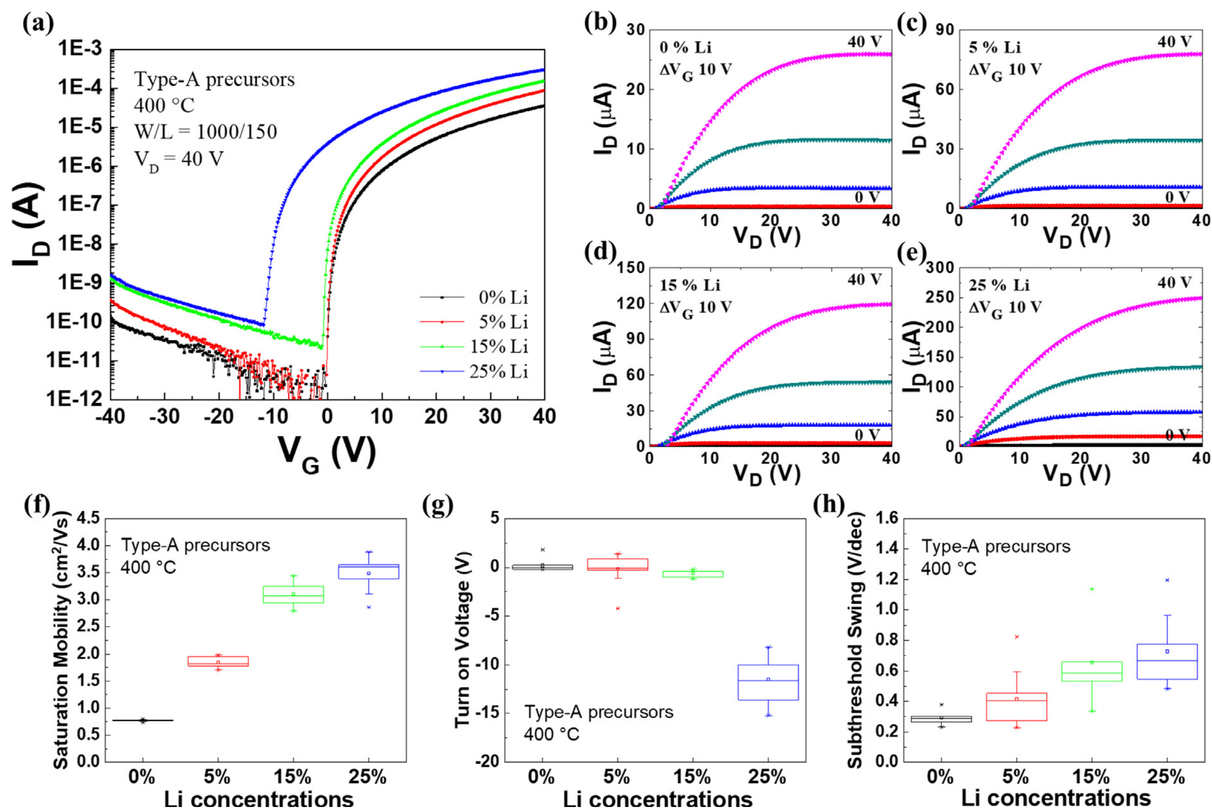

Fig. 3. Electrical characteristics of the Li-IGZO TFTs with type-A precursors. (a) Transfer characteristics with V_D = 40 V. (b) - (e) output characteristics with 0 to 25 % Li doping. The variation in the (f) saturation mobility, (g) turn-on voltage and (h) subthreshold swing of Li-IGZO TFTs as a function of the lithium concentration.

Table 1
Summarized electrical parameters of various Li-IGZO TFTs (type-A; 9 TFTs, saturation region, type-B; 10 TFTs (*8 TFTs), linear region).

Li (%)	Type-A TFTs, 400°C				Type-B TFTs, 350°C			Type-B TFTs, 450°C		
	0	5	15	25	0	5*	10	0	5	10
μ_{FE} (cm^2/Vs)	0.77(σ = 0.02)	1.84(σ = 0.10)	3.11(σ = 0.22)	3.49(σ = 0.33)	0.21(σ = 0.01)	0.47(σ = 0.05)	1.11(σ = 0.15)	0.54(σ = 0.03)	0.91(σ = 0.11)	1.41(σ = 0.07)
log (I_{on}/I_{off})	~ 6.70	~ 7.00	~ 6.48	~ 6.30	~ 5.91	~ 6.60	~ 6.82	~ 6.83	~ 6.75	~ 7.20
V_{on} (V)	0.19(σ = 0.63)	-0.16(σ = 1.73)	-0.62(σ = 0.38)	-11.51(σ = 2.31)	0.35(σ = 2.52)	-1.21(σ = -6.83)	-1(σ = 1.64)	0.7(σ = 1.40)	1(σ = 0.39)	0.48(σ = 0.21)
S.S (V/dec)	0.29(σ = 0.05)	0.41(σ = 0.19)	0.65(σ = 0.28)	0.72(σ = 0.23)	0.60(σ = 0.25)	0.50(σ = 0.16)	0.36(σ = 0.07)	0.47(σ = 0.11)	0.46(σ = 0.04)	0.30(σ = 0.04)

To investigate other characteristics between the IGZO and Li-IGZO films, we also analyzed the XPS spectra of the Li-IGZO thin-films. Fig. 2 shows the oxygen binding energy of the Li-IGZO thin films with various Li concentration using type-A precursors. From the oxygen 1s peak in XPS spectra, there are some distinguishable difference between un-doped and Li-IGZO film. The O1s peaks were fitted with three Gaussian peaks centered near 529.4, 530.2 and 531.3 eV, reflecting the different binding states of oxygen. The sub-peak centered at the 529.4 eV (O−M) is typically associated with the O^{2-} ions present in a stoichiometric IGZO structure without oxygen vacancies. The second peak at the 530.2 eV (O_V) arises from the oxygen bonds with oxygen vacancies. The last peak at the 531.3 eV (O−H) has been reported as the oxygen bonding in the hydroxide (O−H) bonding [14,30–32]. Compared to the IGZO film, the area ratio of O^{2-} ions in oxygen vacancies regions (O_V) were obviously decreased in Li-IGZO films. While the area ratio of oxygen vacancies peak (O_V) is 19 % in the IGZO films, the oxygen vacancies peak area ratio is 7 %, 9 % and 12 % for 5 %, 15 % and 25 % Li doping concentration, respectively. Especially in the 5 % of Li doping, the oxygen vacancies (O_V) apparently decreased from 19 % (IGZO film) to 7 % (5 % Li doped IGZO film). The oxygen vacancies and surface absorbed oxygen is related to charge trapping and the electrical unstable behavior of IGZO TFTs [33]. In addition, we also confirmed that the metal-oxide bonding (O−M) increased in Li-IGZO films. The XPS spectra result indicates that Li doping plays an important role to improve the electrical characteristic of solution-processed IGZO TFTs due to reduced oxygen vacancies and enhanced metal oxide bonding in the IGZO film.

Fig. 3(a) shows the transfer curves of the IGZO TFT (type-A) with various Li doping concentration in saturation region (V_D = 40 V). From the transfer curve in Fig. 3(a) the electrical parameters such as mobility and subthreshold slope could be extracted. From transfer curve of IGZO TFTs made of the type-A precursor solution, the extracted saturation mobility (μ_{sat}) and the current on/off ratio (I_{on}/I_{off}) values were about 0.77 cm^2/Vs and ~ 5 × 10^6 respectively. The turn on voltage (V_{on}) which is defined at gate voltage of initial sharp rise onset in drain current in a log (I_D) versus V_D transfer curve, was 0.19 V. The 5 % Li doped IGZO TFTs showed the saturation mobility of 1.84 cm^2/Vs with an I_{on}/I_{off} ratio of ~1 × 10^7. From this result, we can see the increased saturation mobility and I_{on}/I_{off} ratio with 5 % Li doping. Similarly, the case of 15 and 25 % Li doped IGZO TFT has enhanced saturation mobility of 3.11 and 3.49 cm^2/Vs with an I_{on}/I_{off} ratio of ~3 × 10^6 and ~2 × 10^6, respectively. This improvement in saturation mobility of TFTs is associated with the fewer oxygen deficiencies and reduced carrier concentration [34]. The turn on voltage was slightly negative shifted with increased Li concentration up to 15 % Li doping and especially 25 % Li doping caused significantly turn-on voltage shift in a negative direction. Fig. 3(f), (g) and (h) showed the variation of detailed electrical parameters and they are summarized in Table 1.

To investigate the Li doping effect on IGZO TFT stability, gate bias stress testing was carried out at room temperature in the dark box in air. The positive and negative gate bias stress testing was applied over a 1000 s by holding V_G = 20 V and -20 V, respectively. The evolution of the transfer curve of un-doped and 5 % Li doped IGZO TFT under negative bias stress and its recovery behavior are shown in Fig. 4(a) and (b). During the negative bias stress, there are same turn-on voltage shifts (ΔV_{on} = - 1 V) for both TFTs. The inset of Fig. 4(a) and (b) shows similar turn-on voltage shift under its recovery of the transfer curve toward the initial state. While the negative gate bias stress did not show any difference, the positive gate bias stress causes a different turn-on voltage shift in un-doped and Li doped IGZO TFTs. Fig. 4(c) and (d) shows that the turn-on voltage shifts of the transfer curve of un-doped and 5 % Li doped IGZO TFTs under positive gate bias stress. Positive turn-on voltage shifts was observed with of 16.4 V for un-doped TFTs, while the 5% Li doped IGZO TFTs showed 12.2 V shift. In case of its recovery behavior, Li-IGZO TFTs recovered to initial state faster than un-doped ones.

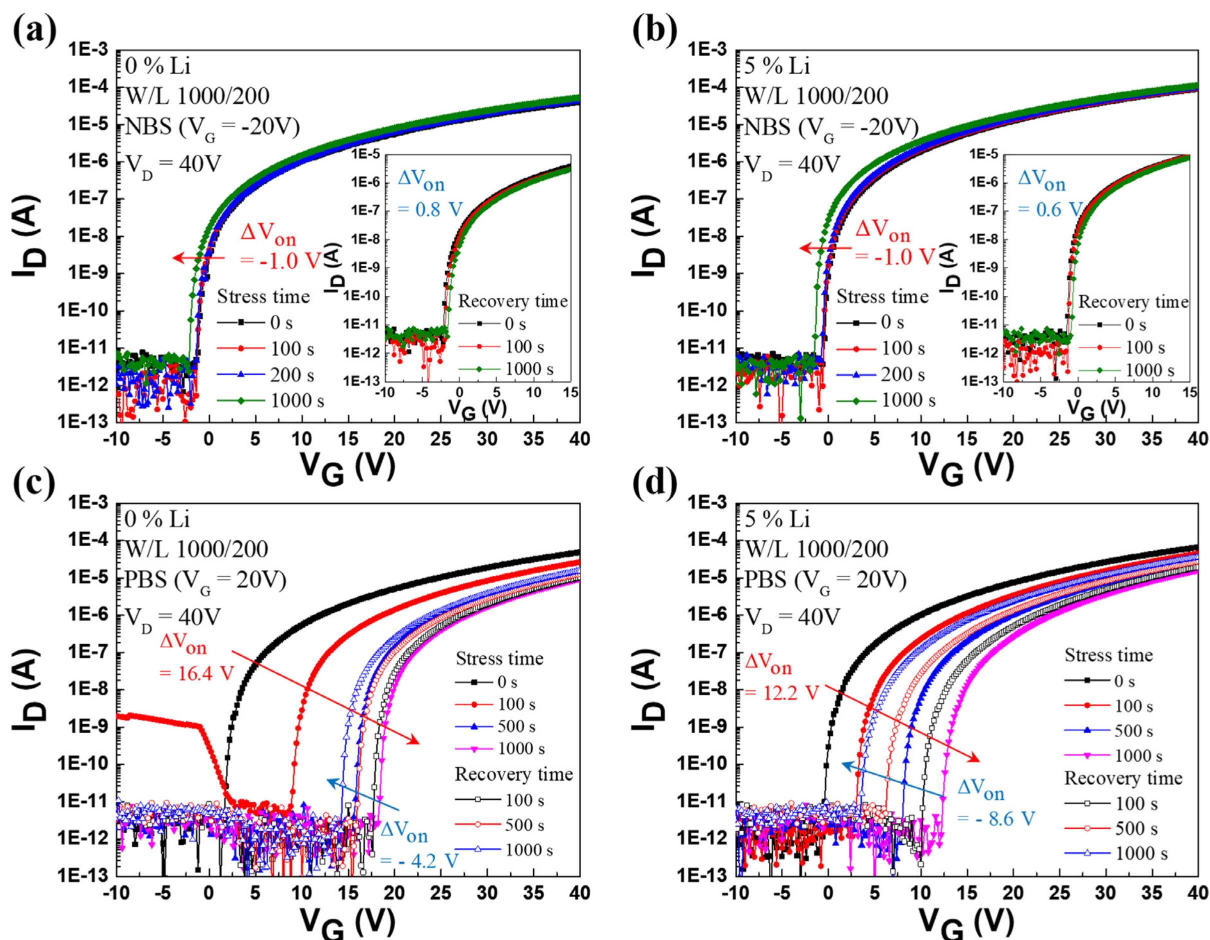

Fig. 4. The evolution of the transfer characteristics of TFTs with increasing NBS / PBS time and its recovery time. (a) IGZO and (b) 5 % lithium doped IGZO TFTs under negative bias stress (V_G = - 20 V, V_D = 0 V). (c) IGZO and (d) 5 % Li doped IGZO TFTs under positive bias stress (V_G = + 20 V, V_D = 0 V).

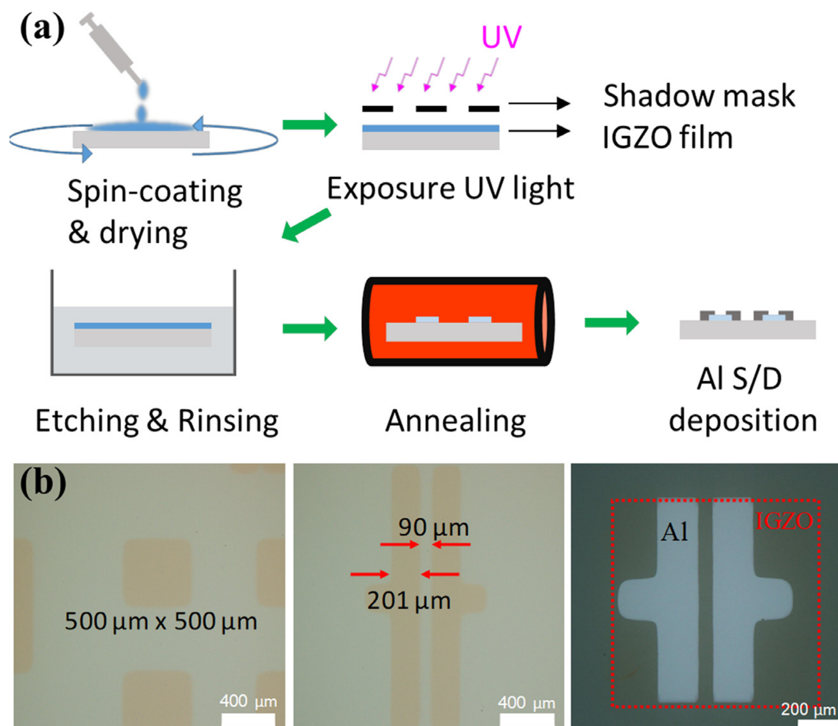

Fig. 5. (a) A Schematic of the fabrication process for UV photo-patterned and Li-IGZO TFTs with type-B precursors and (b) Optical micrographs of patterned IGZO thin films and TFT.

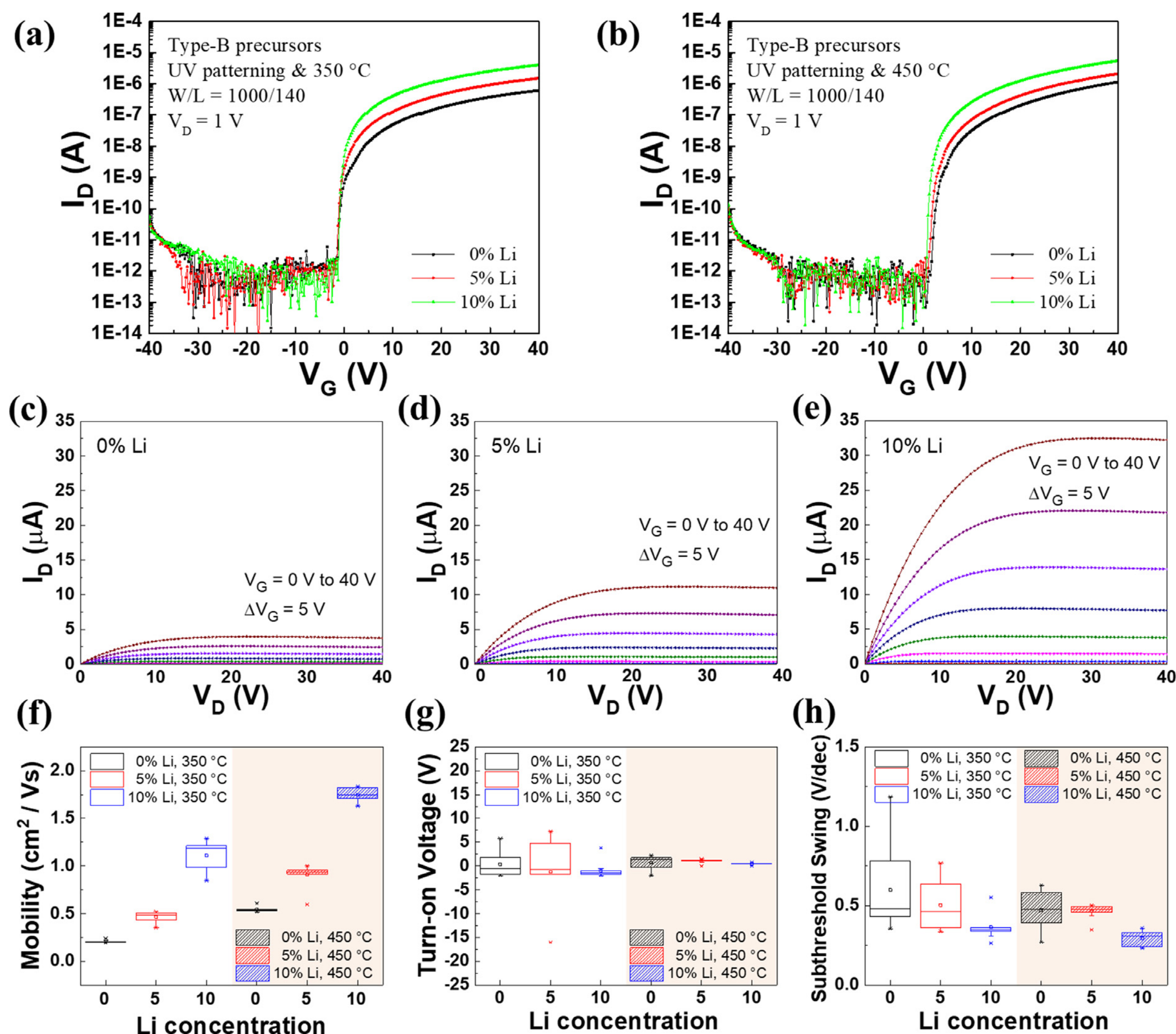

Fig. 6. Electrical characteristics of the UV photo-patterned Li-IGZO TFTs with type-B precursors. Transfer characteristics with annealed at (a) 350 °C and (b) 450 °C under V_D = 1 V. Output characteristics of IGZO TFTs annealed at 450 °C with various Li concentration; (c) 0 %, (d) 5 % and (e) 10 %. The variation in the (f) field effect mobility, (g) turn-on voltage and (h) subthreshold swing of Li-IGZO TFTs as a function of the Li concentration.

We also fabricated Li-IGZO TFTs with UV photo-patterned oxide semiconductor layer by using type-B precursor solutions. When exposed to UV light, observed UV energy enhance chemical formation, making the oxide semiconductor layer resistant to methanol and acetic acid mixture, and thus the oxide thin films can be patterned [19,20]. It is noted that Li-IGZO TFTs fabricated with both type-A and type-B precursors showed similar device performances and behavior tendency with Li doping amount. The experimental procedure of the UV photo-patterned Li-IGZO TFTs is illustrated in Fig. 5(a) and the optical image of patterned IGZO films and TFTs are shown in Fig. 5(b). We could obtain the desired pattern size and space through the shadow metal mask. The transfer characteristics of UV photo-patterned Li-IGZO TFTs at a drain voltage of 1 V are shown in Fig. 6(a) and (b) with annealing temperature 350 °C and 450 °C, respectively. The extracted electrical parameters are shown in Fig. 6(c), (d), and (e). As the Li concentration increases up to 10 %, the mobility of the Li-IGZO TFTs increased. The un-doped IGZO TFTs annealed at 350 °C has a low field effect mobility (μ_{FE}) of 0.21 cm^2/Vs and a logarithmic on/off current ratio ~5.91. However, the addition of small amounts of Li to the IGZO film with low annealing temperature (350 °C) results in significant increases in the μ_{FE}. For examples, 5% and 10% Li doped IGZO TFTs has μ_{FE} of 0.47 and 1.11 cm^2/Vs with higher current on/off ratio than un-doped IGZO TFTs, respectively. As mentioned before in the experimental section, hysteresis behavior of Li-IGZO TFTs was much reduced in comparison with the un-doped ones. The extracted electrical parameters are summarized in Table 1.

4. Conclusions

We demonstrated solution-processed Li doped IGZO TFTs with UV photo-patterned oxide semiconductor layer. From XPS results, appropriate Li doping on IGZO films decreased oxygen vacancies and increased metal oxide bonding. However, Li doping did not affect the amorphous phase of the IGZO film unlike Li doped ZnO films [13]. Electrical characteristics of Li-IGZO TFTs showed the improved mobility and positive bias stress stability. In addition, its recover behavior toward pre-stress state is faster than un-doped IGZO TFTs. We also confirmed that field effect mobility was enhanced as increasing Li concentration. We patterned the Li-IGZO thin films using a simple UV photo-patterning process without degradation of electrical performance. Therefore, we believe that both alkali metal doping and in-situ UV photo-patterning process can be easily applied to other types of oxide and/or alkali metal doped oxide TFTs.

CRediT authorship contribution statement

Jongsu Jang: Conceptualization, Methodology, Formal analysis, Investigation, Writing - original draft, Visualization. **Yongtaek Hong:** Writing - review & editing, Supervision.

Declaration of Competing Interest

The authors declare that they have no known competing financial interests or personal relationships that could have appeared to influence the work reported in this paper.

Acknowledgements

This work was supported by the financial support from the R&D Convergence Program of NST (National Research Council of Science & Technology) of Republic of Korea (CAP-15-04-KITECH).

References

[1] K. Nomura, H. Ohta, A. Takagi, T. Kamiya, M. Hirano, H. Hosono, Room-temperature fabrication of transparent flexible thin-film transistors using amorphous oxide semiconductors, Nature 432 (2004) 488–492, https://doi.org/10.1038/nature03090.
[2] E. Fortunato, P. Barquinha, R. Martins, Oxide semiconductor thin-film transistors: a review of recent advances, Adv. Mater. 24 (2012) 2945–2986, https://doi.org/10.1002/adma.201103228.
[3] C.H. Jung, D.J. Kim, Y.K. Kang, D.H. Yoon, Transparent amorphous In–Ga–Zn–O thin film as function of various gas flows for TFT applications, Thin Solid Films 517 (2009) 4078–4081, https://doi.org/10.1016/j.tsf.2009.01.166.
[4] H. Kumomi, K. Nomura, T. Kamiya, H. Hosono, Amorphous oxide channel TFTs, Thin Solid Films 516 (2008) 1516–1522, https://doi.org/10.1016/j.tsf.2007.03.161.
[5] H.S. Kim, P.D. Byrne, A. Facchetti, T.J. Marks, High performance solution-processed indium oxide thin-film transistors, J. Am. Chem. Soc. 130 (2008) 12580–12581, https://doi.org/10.1021/ja804262z.
[6] T. Kamiya, K. Nomura, H. Hosono, Present status of amorphous In–Ga–Zn–O thin-film transistors, Sci. Technol.Adv. Mater. 11 (2010) 044305, , https://doi.org/10.1088/1468-6996/11/4/044305.
[7] J.H. Park, W.J. Choi, S.S. Chae, J.Y. Oh, S.J. Lee, K.M. Song, H.K. Baik, Structural and electrical properties of solution-processed gallium-doped indium oxide thin-film transistors, Jpn. J. Appl. Phys. 50 (2011) 080202, , https://doi.org/10.1143/JJAP.50.080202.
[8] W.H. Jeong, G.H. Kim, H.S. Shin, B. Du Ahn, H.J. Kim, M.-K. Ryu, K.-B. Park, J.-B. Seon, S.Y. Lee, Investigating addition effect of hafnium in InZnO thin film transistors using a solution process, Appl. Phys. Lett. 96 (2010) 093503, , https://doi.org/10.1063/1.3340943.
[9] J.H. Park, Y.B. Yoo, K.H. Lee, W.S. Jang, J.Y. Oh, S.S. Chae, H.K. Baik, Low-temperature, high-performance solution-processed thin-film transistors with peroxo-zirconium oxide dielectric, ACS Appl. Mater. Interfaces 5 (2013) 410–417, https://doi.org/10.1021/am3022625.
[10] Y.B. Yoo, J.H. Park, K.M. Song, S.J. Lee, H.K. Baik, Non-hydrolytic ester-elimination reaction and its application in solution-processed zinc tin oxide thin film transistors, J. Sol-Gel Sci. Technol. 64 (2012) 257–263, https://doi.org/10.1007/s10971-012-2832-5.
[11] P. Vanysek, Electrochemical series, CRC Handbook Chem. Phys. 8 (2000).
[12] G. Srinivasan, R.R. Kumar, J. Kumar, Li doped and undoped ZnO nanocrystalline thin films: a comparative study of structural and optical properties, J. Sol-Gel Sci. Technol. 43 (2007) 171–177, https://doi.org/10.1007/s10971-007-1574-2.
[13] P.K. Nayak, J. Jang, C. Lee, Y. Hong, Effects of Li doping on the performance and environmental stability of solution processed ZnO thin film transistors, Appl. Phys. Lett. 95 (2009) 193503, , https://doi.org/10.1063/1.3262956.
[14] K.H. Lim, K. Kim, S. Kim, S.Y. Park, H. Kim, Y.S. Kim, UV–visible spectroscopic analysis of electrical properties in alkali metal-doped amorphous zinc tin oxide thin-film transistors, Adv. Mater. 25 (2013) 2994–3000, https://doi.org/10.1002/adma.201204236.
[15] M.-C. Nguyen, M. Jang, D.-H. Lee, H.-J. Bang, M. Lee, J.K. Jeong, H. Yang, R. Choi, Li-assisted low-temperature phase transitions in solution-processed indium oxide films for high-performance thin film transistor, Sci. Rep. 6 (2016) 25079, https://doi.org/10.1038/srep25079.
[16] J.H. Park, J.Y. Oh, H.K. Baik, T.I. Lee, Lithium ion assisted hydration of metal ions in non-aqueous sol–gel inks for high performance metal oxide thin-film transistors, J. Mater. Chem. C 3 (2015) 6276–6283, https://doi.org/10.1039/c5tc00341e.
[17] I.-H. Cho, H.-W. Park, K.-B. Chung, C.-J. Kim, B.-H. Jun, Influence of lithium doping on the electrical properties and ageing effect of ZnSnO thin film transistors, Semicond. Sci. Technol. 33 (2018) 085004, , https://doi.org/10.1088/1361-6641/aacbe3.
[18] T. Zhao, C. Zhao, J. Zhang, I.Z. Mitrovic, E.G. Lim, L. Yang, T. Song, C. Zhao, Enhancement on the performance of eco-friendly solution-processed InO/AlO thin-film transistors via lithium incorporation, J. Alloys Compod. 829 (2020) 154458, , https://doi.org/10.1016/j.jallcom.2020.154458.
[19] Y.-H. Kim, J.-S. Heo, T.-H. Kim, S. Park, M.-H. Yoon, J. Kim, M.S. Oh, G.-R. Yi, Y.-Y. Noh, S.K. Park, Flexible metal-oxide devices made by room-temperature photochemical activation of sol–gel films, Nature 489 (2012) 128–132, https://doi.org/10.1038/nature11434.
[20] J.W. Jo, K.H. Kim, J. Kim, S.G. Ban, Y.H. Kim, S.K. Park, High-mobility and hysteresis-free flexible oxide thin-film transistors and circuits by using bilayer sol-gel gate dielectrics, ACS Appl. Mater. Interfaces 10 (2018) 2679–2687, https://doi.org/10.1021/acsami.7b10786.
[21] Y.S. Rim, H. Chen, Y. Liu, S.-H. Bae, H.J. Kim, Y. Yang, Direct light pattern integration of low-temperature solution-processed all-oxide flexible electronics, ACS Nano 8 (2014) 9680–9686, https://doi.org/10.1021/nn504420r.
[22] S. Sanctis, R.C. Hoffmann, M. Bruns, J.J. Schneider, Direct photopatterning of solution–processed amorphous indium zinc oxide and zinc tin oxide semiconductors—a chimie douce molecular precursor approach to thin film electronic oxides, Adv. Mater. Interfaces 5 (2018) 1800324, , https://doi.org/10.1002/admi.201800324.
[23] K.-H. Wang, H.-W. Zan, O. Soppera, The zinc-loss effect and mobility enhancement of DUV-patterned sol–gel IGZO thin-film transistors, Semicond. Sci. Technol. (2018) 33, https://doi.org/10.1088/1361-6641/aaa611.
[24] M. Miyakawa, M. Nakata, H. Tsuji, Y. Fujisaki, Simple and reliable direct patterning method for carbon-free solution-processed metal oxide TFTs, Sci. Rep. 8 (2018) 12825, https://doi.org/10.1038/s41598-018-31134-w.
[25] J.-F. Chang, H. Sirringhaus, Patterning of solution-processed semiconducting polymers in high-mobility thin-film transistors by physical delamination, Adv. Mater. 21 (2009) 2530–2535, https://doi.org/10.1002/adma.200803794.
[26] P. Görrn, F. Ghaffari, T. Riedl, W. Kowalsky, Zinc tin oxide based driver for highly transparent active matrix OLED displays, Solid-State Electron. 53 (2009) 329–331, https://doi.org/10.1016/j.sse.2009.01.006.
[27] S.J. Kim, S. Yoon, H.J. Kim, Review of solution-processed oxide thin-film transistors, Japanese J. Appl. Phys. 53 (2014), https://doi.org/10.7567/JJAP.53.02BA02.
[28] K. Kim, S. Park, J.-B. Seon, K.-H. Lim, K. Char, K. Shin, Y.S. Kim, Patterning of flexible transparent thin-film transistors with solution-processed zno using the binary solvent mixture, Adv. Funct. Mater. 21 (2011) 3546–3553, https://doi.org/10.1002/adfm.201100323.
[29] H. Hosono, Ionic amorphous oxide semiconductors: Material design, carrier transport, and device application, J. Non•Cryst. Solids 352 (2006) 851–858, https://doi.org/10.1016/j.jnoncrysol.2006.01.073.
[30] C.Y. Koo, K. Song, Y. Jung, W. Yang, S.-H. Kim, S. Jeong, J. Moon, Enhanced performance of solution-processed amorphous LiYInZnO thin-film transistors, ACS Appl. Mater. Interfaces 4 (2012) 1456–1461, https://doi.org/10.1021/am201701v.
[31] S.M. Sze, K.K. Ng, Physics of Semiconductor Devices, John Wiley & Sons, 2006.
[32] K.-M. Liu, L.F. Register, S.K. Banerjee, Quantum transport simulation of strain and orientation effects in sub-20 nm silicon-on-insulator FinFETs, IEEE Trans. Electron Dev. 58 (2010) 4–10, https://doi.org/10.1109/Ted.2010.2084090.
[33] W.-T. Chen, S.-Y. Lo, S.-C. Kao, H.-W. Zan, C.-C. Tsai, J.-H. Lin, C.-H. Fang, C.-C. Lee, Oxygen-dependent instability and annealing/passivation effects in amorphous In–Ga–Zn–O thin-film transistors, IEEE Electron. Dev. Lett. 32 (2011) 1552–1554, https://doi.org/10.1109/led.2011.2165694.
[34] B.-Y. Su, S.-Y. Chu, Y.-D. Juang, S.-Y. Liu, Effects of Mg doping on the gate bias and thermal stability of solution-processed InGaZnO thin-film transistors, J. Alloys Compd. 580 (2013) 10–14, https://doi.org/10.1016/j.jallcom.2013.05.077.